Cumulant expansions for measuring water exchange using diffusion MRI

Lipeng Ning,[1,a)] Markus Nilsson,[2] Samo Lasič,[3] Carl-Fredrik Westin,[1] and Yogesh Rathi[1]
[1]*Brigham and Women's Hospital, Harvard Medical School, Boston, Massachusetts 02215, USA*
[2]*Lund University, Lund, Sweden*
[3]*CR Development, AB, Lund, Sweden*

(Received 14 November 2017; accepted 24 January 2018; published online 21 February 2018)

The rate of water exchange across cell membranes is a parameter of biological interest and can be measured by diffusion magnetic resonance imaging (dMRI). In this work, we investigate a stochastic model for the diffusion-and-exchange of water molecules. This model provides a general solution for the temporal evolution of dMRI signal using any type of gradient waveform, thereby generalizing the signal expressions for the Kärger model. Moreover, we also derive a general *n*th order cumulant expansion of the dMRI signal accounting for water exchange, which has not been explored in earlier studies. Based on this analytical expression, we compute the cumulant expansion for dMRI signals for the special case of single diffusion encoding (SDE) and double diffusion encoding (DDE) sequences. Our results provide a theoretical guideline on optimizing experimental parameters for SDE and DDE sequences, respectively. Moreover, we show that DDE signals are more sensitive to water exchange at short-time scale but provide less attenuation at long-time scale than SDE signals. Our theoretical analysis is also validated using Monte Carlo simulations on synthetic structures. *Published by AIP Publishing.* https://doi.org/10.1063/1.5014044

I. INTRODUCTION

Diffusion magnetic resonance imaging (dMRI) is widely used to probe microstructure of cells and permeability of porous media via the diffusive motion of water molecules.[1–4] A common approach for measuring water exchange using dMRI is to apply Kärger's model[5] to fit the dMRI signal measured by the standard Stejskal-Tanner sequence,[6] here referred to as the single diffusion encoding (SDE) sequence.[7] In the Kärger model, molecular motion in different tissue compartments is modeled by free diffusion with different diffusion coefficients. Molecules are assumed to have a stationary probability to jump between compartments. This oversimplified assumption ignores the dependence of location on exchange of molecules but can be justified when the exchange is "barrier limited."[8,9] This means that molecules within each compartment are well mixed, as diffusion is faster than the exchange so that the dependence of exchange on location can be neglected.

Exchange measurements using the Kärger model were originally proposed only for SDE sequences,[5] but later studies suggested benefits of double diffusion encoding (DDE) sequences.[10,11] Recently, the DDE-based filter exchange imaging (FEXI) technique was proposed to enable *in vivo* imaging of exchange rates on clinical MRI scanners.[12] The FEXI approach provides an apparent exchange rate (AXR) sensitive to tissue permeability and has been applied to study human brain tissue,[13] brain tumors,[14] breast cancer,[15] and kidney.[16] However, the AXR can be sensitive to deviations from the idealised DDE experiment arising due to, for example, imaging gradients.[17] Moreover, there are no theoretical guidelines available for selecting the optimal experimental parameters, although some work has been done using numerical optimization techniques.[14] Furthermore, the difference between FEXI and standard SDE and DDE sequences has not been thoroughly analyzed.

To overcome these limitations, we propose a general approach for modeling the dMRI signal in a diffusion-and-exchange system. Our method accepts any type of gradient waveform and is developed based on a stochastic differential equation that provides a probability distribution of the diffusion-and-exchange process of molecules. As a result of this stochastic model, we derive a generalized model to characterize the temporal evolution of dMRI signal under any type of gradient waveform. This general model reduces to the standard Kärger's model in the special case of SDE sequences. We also derive the cumulant expansion of the dMRI signal for any type of sequence accounting for water exchange. Based on the cumulant expansion, we compare the dMRI signal from SDE and DDE sequences and design the optimal parameters for different sequences under constraints on the maximal b-value and diffusion time. We also derive an explicit expression for the special case of the FEXI sequence. Monte Carlo simulations show excellent agreement with our theoretical results.

II. THEORY

A. Modeling of diffusion-and-exchange processes

Our approach for modeling the dMRI signal due to diffusion and exchange of molecules in a multi-compartment

[a)]Author to whom correspondence should be addressed: lning@bwh.harvard.edu. Telephone: 617-525-6024. Fax: 617-525-6214.

system uses the following stochastic differential equation:

$$d\boldsymbol{x}_t = \sigma(\boldsymbol{x}_t)d\boldsymbol{w}_t, \tag{1}$$

where $\boldsymbol{x}_t \in \mathbb{R}^3$ denotes the location of a water molecule and $\boldsymbol{w}_t$ represents the standard Wiener process with $d\boldsymbol{w}_{t_1}$ and $d\boldsymbol{w}_{t_2}$ being independent Gaussian random variables if $t_1 \neq t_2$ with covariance given by

$$\mathcal{E}(d\boldsymbol{w}_t d\boldsymbol{w}_t') = Idt,$$

where $\boldsymbol{a}'$ denotes the transpose of a vector $\boldsymbol{a}$, I denotes the identity matrix of size 3×3, and $\sigma(\boldsymbol{x}_t)$ represents the variance of $d\boldsymbol{x}_t$. Throughout this paper, boldface small letters, e.g., $\boldsymbol{w}$, $\boldsymbol{a}$, represent vector-valued variables. We assume that the variance is isotropic, i.e., $\sigma(\boldsymbol{x}_t) \in \mathbb{R}$, to simplify notations, though the results of this paper can be extended in a straightforward manner to a more general setting when $\sigma(\boldsymbol{x}_t)$ is matrix-valued. Thus, the covariance of the increment $d\boldsymbol{x}_t$ is given by $\mathcal{E}(d\boldsymbol{x}_t d\boldsymbol{x}_t') = \sigma^2(\boldsymbol{x}_t)Idt$. Moreover, the location $\boldsymbol{x}_t$ of a molecule is also characterized by a state $s(\boldsymbol{x}_t) \in \{1, 2\}$, which determines the value of $\sigma(\boldsymbol{x})$. To simplify notations, we denote $s(\boldsymbol{x}_t)$ by $s(t)$. Moreover, we assume that

$$\sigma(\boldsymbol{x}_t)^2 = \begin{cases} 2D_1, & \text{if } s(t) = 1, \\ 2D_2, & \text{if } s(t) = 2, \end{cases}$$

where $D_1 \neq D_2$ and they represent the scalar-valued diffusion coefficients for the two compartments, respectively.

An important assumption we have made in all our derivations above is that the diffusivity is constant (time-invariant) at the experimental time scale being used in this work. Such an assumption is well-founded as the apparent diffusion coefficient (ADC) has very pronounced time-dependence only at short time scales and converges to the "bulk" diffusion coefficient D_∞ at long time scales.[18] Recent studies[19] also show very slowly varying or constant diffusivity at long time scale in biological tissue. Since exchange occurs at long time scale, the diffusion coefficient can be assumed to be constant. The two diffusion coefficients, D_1 and D_2, represent the long-time diffusive motion of water molecules in two structures, e.g., intra- and extra-cellular spaces. In situations where the time scale for the exchange is short, restrictions and hindrances induced time-varying diffusivity needs to be considered.[20–22] In this case, a more realistic model, such as the Ornstein-Uhlenbeck model,[23,24] can be used for modeling the two types of diffusive motions. But, we will only focus on Eq. (1) in this paper. Alternatively, a Langevin equation with fluctuating diffusivity was assumed to switch between two constant states.[25,26] Here, we propose a different approach from Refs. 25 and 26 for modeling the switch between states so that the signal expression is consistent with Kärger's model.

We model the exchange of molecules between the two compartments by a probabilistic change in $s(t)$. In particular, the state of a molecule is to be described by a probability vector $\boldsymbol{p}(t) := [p_1(t), p_2(t)]'$ with $p_i(t)$ being the probability of $s(t) = i$. For a molecule with $s(0) = 1$, the probability vector is given by $\boldsymbol{p}(0) = [1, 0]' =: \boldsymbol{e}_1$. Similarly, $\boldsymbol{p}(0) = [0, 1]' =: \boldsymbol{e}_2$ corresponds to a molecule with $s(0) = 2$. Due to exchange, the probability distribution evolves according to the following differential equation:

$$\frac{d}{dt}\boldsymbol{p}(t) = K\boldsymbol{p}(t), \tag{2}$$

where the matrix K is given by

$$K := \begin{bmatrix} -k_{12} & k_{21} \\ k_{12} & -k_{21} \end{bmatrix}.$$

The total mass, i.e., $p_1(t) + p_2(t)$, is assumed to be time-invariant. The probability distribution for molecules with initial states $\boldsymbol{e}_1$ and $\boldsymbol{e}_2$ is given by the two columns of the following matrix:

$$\begin{aligned} \exp(Kt) &= \begin{bmatrix} p_{11}(t) & p_{21}(t) \\ p_{12}(t) & p_{22}(t) \end{bmatrix} \\ &= \begin{bmatrix} p_1^\infty + p_2^\infty e^{-kt} & p_1^\infty(1 - e^{-kt}) \\ p_2^\infty(1 - e^{-kt}) & p_2^\infty + p_1^\infty e^{-kt} \end{bmatrix}, \end{aligned}$$

where $p_1^\infty = \frac{k_{21}}{k_{12}+k_{21}}$, $p_2^\infty = \frac{k_{12}}{k_{12}+k_{21}}$, and $k = k_{12} + k_{21}$ with $k_{12}, k_{21} \geq 0$ being the exchange rate between the two compartments. The probability vector $\boldsymbol{p}^\infty = [p_1^\infty, p_2^\infty]'$ is the stationary value of (2), which implies that the stationary fractions of molecules in the two compartments are p_1^∞ and p_2^∞, respectively.

B. The diffusion-exchange model

Let $\boldsymbol{g}(t)$ with $t \in [0, T]$ denote the vectorial gradient sequence. Then the phase change of a diffusing molecule due to the gradient sequence is given by

$$\phi(T) = \int_0^T \gamma \boldsymbol{g}(t)'\boldsymbol{x}_t dt = -\int_0^T \boldsymbol{q}(t)'\sigma(\boldsymbol{x}_t)d\boldsymbol{w}_t,$$

where γ denotes the gyromagnetic ratio, $\boldsymbol{q}(t) = \int_0^t \gamma \boldsymbol{g}(t_1)dt_1$, which is assumed to satisfy the spin-echo condition, i.e., $\boldsymbol{q}(T) = 0$. Moreover, we decompose $\boldsymbol{q}(t) = q(t)\boldsymbol{n}(t)$ with $q(t)$ being a scalar and $\boldsymbol{n}(t)$ being a unit vector. Then,

$$\phi(T) = -\int_0^T q(t)\sigma(\boldsymbol{x}_t)dw_t, \tag{3}$$

where $w_t = \boldsymbol{n}(t)'\boldsymbol{w}_t$ is a scalar-valued Wiener process. The diffusion MRI signal at time T is given by the expected value $S(q, T) := \mathcal{E}(e^{\mathrm{i}\phi(T)})$, where $\mathrm{i} = \sqrt{-1}$, with respect to the probability distribution of $\phi(T)$ from all molecules.

Let $S_i(q, t)$ for $i \in \{1, 2\}$ denote the fraction of dMRI signal from all molecules with state $s(t) = i$ at time t, i.e.,

$$S_i(q, t) = \sum_{j=1}^{2} p_j p_{ji}(t)\mathcal{E}(e^{\mathrm{i}\phi(t)} \mid s(t) = i, s(0) = j).$$

Then, the dMRI signal from all molecules is given by

$$S(q, t) = S_1(q, t) + S_2(q, t). \tag{4}$$

As a generalization of the signal expression for the standard Kärger's model, we show that the temporal evolution of $S_i(q, t)$ for $t \in [0, T]$ that is consistent with Eqs. (1) and (2) is given by the following equation:

$$\begin{bmatrix} \frac{\partial S_1(q,t)}{\partial t} \\ \frac{\partial S_2(q,t)}{\partial t} \end{bmatrix} = \begin{bmatrix} -q^2(t)D_1 - k_{12} & k_{21} \\ k_{12} & -q^2(t)D_2 - k_{21} \end{bmatrix} \begin{bmatrix} S_1(q,t) \\ S_2(q,t) \end{bmatrix}. \tag{5}$$

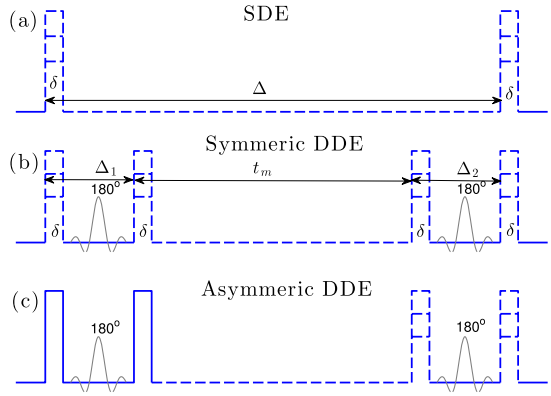

FIG. 1. An illustration of three types of gradient sequences: (a) A standard SDE sequence with variable diffusion time and magnitude; (b) a symmetric DDE sequence with two symmetric pairs of pulses, where the diffusion time Δ_1, Δ_2 and the magnitude of the two pairs of pulses are identical, i.e., $\Delta_1 = \Delta_2$, $q_1 = q_2$, and the mixing time t_m and q_a are variable parameters; (c) an asymmetric DDE sequence, similar to the FEXI sequence in Ref. 12, where the magnitude for the first pair of pulses is fixed (indicated by solid lines), the diffusion time $\Delta_1 = \Delta_2$, and the mixing time and the magnitude of the second pair of pulses are variable.

The proof of Eq. (5) is provided in Appendix A. We note that in the special case of SDE experiment with narrow pulse, $q^2(t)$ is constant, in which case Eq. (5) becomes the standard Kärger's model.[5] The derivation leading to Eq. (5) is one of the contributions of the present work.

The dMRI signal in Eq. (4) can be obtained from the solution to Eq. (5). In the special case of SDE or DDE experiment with narrow pulse, $q^2(t)$ is either constant or piecewise constant, which leads to a closed-form solution to Eq. (5). Specifically, let $K := \begin{bmatrix} -k_{12} & k_{21} \\ k_{12} & -k_{21} \end{bmatrix}$, and $M(q) := K - Dq^2$ with $D = \begin{bmatrix} D_1 & 0 \\ 0 & D_2 \end{bmatrix}$. Then the dMRI signal obtained using a SDE sequence with narrow pulse, as shown in Fig. 1(a), is given by

$$S_{\mathrm{SDE}}(q, T) = \mathbf{1}' \exp\left(M(q)T\right)\boldsymbol{p}^{\infty}, \tag{6}$$

which is also the solution by Kärger,[5] where q denotes the constant q-value, $\exp(A)$ denotes the matrix exponential function of a matrix A, $\mathbf{1}$ denotes a vector whose entries are all equal to one. For a DDE sequence with narrow pulse, as shown in Fig. 1(b), we denote the q-value between the first and second pair of pulses as q_1 and q_2, respectively, i.e., $q(t) = q_1$ for $t \in [0, \Delta_1]$ and $q(t) = q_2$ for $t \in [T - T_2, T]$, where $T = \Delta_1 + \Delta_2 + t_m$, with t_m being the mixing time between the two pairs of pulses. Then the dMRI signal obtained for a DDE sequence is given by

$$\begin{aligned} S_{\mathrm{DDE}}(q_1, q_2, \Delta_1, \Delta_2, t_m) = \mathbf{1}' \exp\left(M(q_2)\Delta_2\right) \exp\left(Kt_m\right) \\ \times \exp\left(M(q_1)\Delta_1\right)\boldsymbol{p}^{\infty}. \end{aligned} \tag{7}$$

For completeness, we provide the closed-form expression for the matrix exponential $\exp(M(q)T)$ in Appendix B. In the more general case when $q(t)$ is a continuous function of t, there is in general no closed-form solution for Eq. (5).

C. On the cumulant expansion with water exchange

Although the expressions in Eqs. (6) and (7) can be directly used to model SDE and DDE signals with given experimental parameters, the complex expression of matrix exponentials is a major limitation to gain insights about choosing the optimal experimental parameters, especially for DDE sequences, which are characterized by multiple parameters such as diffusion time, mixing time, and gradient strength. A common approach to simplify the dMRI signal model and to gain insights about the role of experimental parameters is to use the cumulant expansion[27] expressed as follows:

$$\begin{aligned} \ln S(q, T) = \mathrm{i}\langle\phi(T)\rangle_c - \frac{1}{2}\langle\phi(T)^2\rangle_c - \frac{\mathrm{i}}{6}\langle\phi(T)^3\rangle_c \\ + \frac{1}{24}\langle\phi(T)^4\rangle_c + \cdots, \end{aligned}$$

where the cumulant moments $\langle\phi(T)^n\rangle_c$ can be expressed in terms of ordinary moments $\mathcal{E}(\phi(T)^n)$. Typically, the probability distribution function of $\phi(T)$ is assumed to be symmetric. As a result, all the odd order moments $\mathcal{E}(\phi(T)^{2n-1})$ are equal to zero. The second and fourth order cumulant moments are given by

$$\langle\phi(T)^2\rangle_c = \mathcal{E}(\phi(T)^2), \tag{8}$$

$$\langle\phi(T)^4\rangle_c = \mathcal{E}(\phi(T)^4) - 3\mathcal{E}(\phi(T)^2)^2, \tag{9}$$

respectively. Since the expression for the dMRI signal in SDE and DDE experiments is known, a general approach for computing the cumulant moments is to compute the Taylor-series expansion of S or $\ln S$. But the complex expression for the dMRI signal, especially for DDE experiments, makes the derivation of the cumulant expansion extremely tedious. Consequently, we propose a different approach to derive the cumulant expansion by taking advantage of the proposed stochastic diffusion-and-exchange model in Eqs. (1) and (2).

1. On the second-order moment

From Eq. (3), the second order cumulant moment of $\phi(T)$ is given by

$$\begin{aligned} \mathcal{E}(\phi^2(T)) &= \int_0^T \int_0^T q(t_1)q(t_2)\mathcal{E}\left(\sigma(\boldsymbol{x}_{t_1})\sigma(\boldsymbol{x}_{t_2})dw_{t_1}dw_{t_2}\right) \\ &= \int_0^T \int_0^T q(t)^2\mathcal{E}\left(\sigma(\boldsymbol{x}_t)^2\right)dt. \end{aligned} \tag{10}$$

We note that

$$\begin{aligned} \mathcal{E}(\sigma(\boldsymbol{x}_t)^2) &= 2\sum_{i=1}^{2} \mathrm{Prob}(s(t) = i)D_i \\ &= 2(p_1D_1 + p_2D_2) =: 2\bar{D}. \end{aligned}$$

Thus, Eq. (10) is equal to

$$\mathcal{E}(\phi^2(T)) = 2\bar{D}\int_0^T q(t)^2dt = 2\bar{D}b, \tag{11}$$

where the b-value $b := \int_0^T q(t)^2dt$, which is equal to q^2T in SDE experiments and $q_1^2\Delta_1 + q_2^2\Delta_2$ in DDE experiments (under narrow pulse assumption). We remark that Eq. (11) implies that the second order moment does not contain information about the water exchange rate. Moreover, Eq. (11) also

implies that the apparent diffusion coefficient (ADC) is given by

$$\mathrm{ADC} := \frac{\partial \mathcal{E}(\phi^2(T))}{2\partial b}\,|_{b=0} = \bar{D}, \tag{12}$$

which is independent of the type of gradient waveform used. Similarly, one can show that Eq. (12) holds even if there are more than two components in the diffusion-exchange model, as long as the diffusion-exchange processes can be modeled by Eq. (1).

2. On the fourth-order moment

Due to the independence between dw_{t_1} and dw_{t_2} for $t_1 \neq t_2$, the fourth-order moment $\mathcal{E}(dw_{t_1}dw_{t_2}dw_{t_3}dw_{t_4})$ is nonzero only if the set of indices $\{t_1, t_2, t_3, t_4\}$ consists of two pairs of equal values, e.g., $t_1 = t_2$ and $t_3 = t_4$. Thus, we obtain

$$\mathcal{E}(\phi^4(T)) = 3\int_0^T \int_0^T q(t_1)^2 q(t_2)^2 \mathcal{E}(\sigma(\boldsymbol{x}_{t_1})^2 \sigma(\boldsymbol{x}_{t_2})^2) dt_1 dt_2. \tag{13}$$

To compute the correlation $\mathcal{E}(\sigma(\boldsymbol{x}_{t_1})^2\sigma(\boldsymbol{x}_{t_2})^2)$, we assume that $t_1 \leq t_2$. Then,

$$\begin{aligned}
&\mathcal{E}(\sigma(\boldsymbol{x}_{t_1})^2\sigma(\boldsymbol{x}_{t_2})^2) \\
&= p_1^\infty \Big(p_{11}(t_1)p_{11}(t_2-t_1)4D_1^2 + p_{11}(t_1)p_{12}(t_2-t_1)4D_1D_2 \\
&\quad + p_{12}(t_1)p_{21}(t_2-t_1)4D_1D_2 + p_{12}(t_1)p_{22}(t_2-t_1)4D_2^2 \Big) \\
&\quad + p_2^\infty \Big(p_{21}(t_1)p_{11}(t_2-t_1)4D_1^2 + p_{21}(t_1)p_{12}(t_2-t_1)4D_1D_2 \\
&\quad + p_{22}(t_1)p_{21}(t_2-t_1)4D_1D_2 + p_{22}(t_1)p_{22}(t_2-t_1)4D_2^2 \Big) \\
&= 4(p_1^\infty D_1 + p_2^\infty D_2)^2 + 4p_1^\infty p_2^\infty (D_1 - D_2)^2 e^{-k(t_2-t_1)}.
\end{aligned} \tag{14}$$

To further simplify Eq. (13), we define $\mathrm{Var}(D) := p_1^\infty p_2^\infty (D_1 - D_2)^2$, which is equal to the variance of the diffusivities. Then, we introduce the following function:

$$c(t) := \bar{D}^2 + \mathrm{Var}(D)e^{-kt} \tag{15}$$

for $t \in [-T, T]$, which is the autocorrelation function for $\sigma(\boldsymbol{x}_t)^2$ in Eq. (14) scaled by $\frac{1}{4}$. Thus, Eq. (13) can be written as

$$\mathcal{E}(\phi^4(T)) = 12\int_0^T \int_0^T q(t_1)^2 q(t_2)^2 c(|t_1 - t_2|) dt_1 dt_2. \tag{16}$$

Using a similar methodology as in our earlier work,[22,28] we can further simplify the above equation to

$$\mathcal{E}(\phi^4(T)) = 24\int_0^T c(t) q_4(t) dt, \tag{17}$$

where $q_4(t)$ is defined as

$$q_4(t) := \int_0^T q^2(t_1) q^2(t_1 + t) dt_1,$$

where we assume $q(t) = 0$ for $t \geq T$. We note that the fourth-order moment is a function of the exchange rate and the fourth-order autocorrelation function of $q(t)$. For completeness, we provide a general expression for other higher order moments in Appendix C. By applying Eqs. (17) and (11) to Eq. (9), we obtain

$$\langle \phi(T)^4 \rangle_c = 24\mathrm{Var}(D)\int_0^T e^{-kt} q_4(t) dt, \tag{18}$$

which shows the dependence of the fourth-order cumulant on the exchange rate and the gradient sequence.

D. General signal expression

At this point, we can define a signal expression that generalizes across all gradient waveforms

$$\ln S = -\bar{D}b + \frac{1}{2}\mathrm{Var}(D)h(\cdot)b^2 + O(b^3), \tag{19}$$

where $h(\cdot)$ denotes an exchange-sensitivity function of the gradient sequence which is defined by

$$h(\cdot) = 2\int_0^T e^{-kt}\tilde{q}_4(t) dt \tag{20}$$

and

$$\tilde{q}_4(t) = \frac{q_4(t)}{b^2}. \tag{21}$$

The expansion in Eq. (19) is based on the assumption of low b-values so that the third or higher order terms of b are negligible compared to b^2. The term $\tilde{q}_4(t)$ contains the timing information of the gradient waveform. Note that the ability to observe exchange relies on the presence of intra-voxel variance in diffusivity, i.e., $\mathrm{Var}(D) > 0$. Finally, in the absence of exchange, or for very slow exchange where $kT \ll 1$, we get $e^{-kt} \approx 1$ for $0 \leq t \leq T$ and thus $h(\cdot) = 1$. In the presence of exchange, $h(\cdot) < 1$, and in the case of exchange much faster than the gradient waveform, we get $h(\cdot) \to 0$ meaning that the system will appear as a single system without any observable diffusional variance.

Note the similarity of Eq. (19) to the diffusional kurtosis model[29]

$$\ln S \approx -D_{\mathrm{app}}b + \frac{1}{6}D_{\mathrm{app}}^2 K_{\mathrm{app}} b^2, \tag{22}$$

where $D_{\mathrm{app}} = \bar{D}$ in our notation and $K_{\mathrm{app}} = 6\mathrm{Var}(D)/\bar{D}^2$ in the absence of exchange. However, the presence of exchange reduces the apparent kurtosis according to

$$K_{\mathrm{app}}(\cdot) = 3\frac{\mathrm{Var}(D)}{\bar{D}^2}h(\cdot), \tag{23}$$

which depends on the gradient sequences and diffusion time.

1. Defining a generalized exchange weighting time

To further analyze the effect of water-exchange in dMRI signals, we consider the situation when $e^{-kt} \approx 1 - kt$ for $t \in [0, T]$. Then we get

$$\begin{aligned}
h(\cdot) &\approx 2\int_0^T (1 - kt)\tilde{q}_4(t) dt, \\
&= 1 - k\Gamma,
\end{aligned} \tag{24}$$

where we define the exchange weighting time Γ as

$$\Gamma := 2\int_0^T t\tilde{q}_4(t) dt. \tag{25}$$

Accordingly, we have an approximation of Eq. (19) as

$$\ln S \approx -\bar{D}b + \frac{1}{2}\mathrm{Var}(D)(1 - k\Gamma)b^2. \tag{26}$$

In the following, we will compute the function $h(\cdot)$ and the signal model in Eq. (26) for three types of sequences shown in Fig. 1, which includes a standard SDE sequence in Fig. 1(a), a DDE sequence with two identical pairs of pulses in Fig. 1(b) where $\Delta_1 = \Delta_2$, and a FEXI type of DDE sequence in Fig. 1(c) where the magnitude of the first pair of pulses is fixed (indicated by solid lines). Although the signal model for SDE experiments has been well studied in Refs. 1 and 30, comparing the different Γ's will highlight the sensitivity of dMRI signal to water exchange rate for these gradient waveforms.

2. Signal expression for SDE sequences

For the SDE sequence shown in Fig. 1(a), if the pulse width δ is negligibly small, then $h(\cdot)$ is given by

$$h_{\mathrm{SDE}}(\tau) = \frac{2}{\tau} - \frac{2}{\tau^2} + \frac{2}{\tau^2}e^{-\tau}, \tag{27}$$

where $\tau := k\Delta$. The corresponding exchange-weighted time is equal to

$$\Gamma_{\mathrm{SDE}} = \frac{1}{3}\Delta. \tag{28}$$

In the case of finite pulse width, the exchange-weighted time is equal to

$$\Gamma_{\mathrm{SDE}} = \frac{1}{3}f(\delta, \Delta), \tag{29}$$

where

$$f(\delta, \Delta) = (\Delta - \frac{1}{3}\delta)^{-2}(\Delta^3 - \Delta^2\delta + \frac{2}{3}\delta^2\Delta - \frac{4}{21}\delta^3).$$

If $\Delta \gg \delta$, $f(\delta, \Delta) \approx (\Delta - \frac{1}{3}\delta)$ which is equal to the equivalent diffusion time.

3. Signal expression for DDE sequences

First, we consider the narrow-pulse situation when the diffusion time $\Delta_1 = \Delta_2 = \Delta$, $T = 2\Delta + t_m$, and the b-values corresponding to the two pairs of pulses are given by b_1 and b_2, respectively. Following Eq. (18), we obtain

$$h_{\mathrm{DDE_A}}(\cdot) = \frac{b_1^2 + b_2^2}{b^2}h_{\mathrm{SDE}}(\tau_1) + \frac{2b_1b_2}{b^2}h_{\mathrm{DDE}}(\tau_1, \tau), \tag{30}$$

where we define

$$h_{\mathrm{DDE}}(\tau_1, \tau) := \frac{1}{\tau_1^2}(e^{-\tau+2\tau_1} + e^{-\tau} - 2e^{-\tau+\tau_1}),$$

$\tau_1 = k\Delta_1$, $\tau = kT$, $b = b_1 + b_2$, and the subindex $\mathrm{DDE_A}$ denotes the asymmetric DDE sequence. The corresponding exchange-weighted time is equal to

$$\Gamma_{\mathrm{DDE_A}} = \frac{b_1^2 + b_2^2}{3b^2}\Delta_1 + \frac{2b_1b_2}{b^2}(\Delta_1 + t_m).$$

In the special case when $b_1 = b_2$, the corresponding exchange weighting time is

$$\Gamma_{\mathrm{DDE_S}} = \frac{2}{3}\Delta_1 + \frac{1}{2}t_m.$$

The exchange weighting time can be generalized to the situation when the pulse width is finite as follows:

$$\begin{aligned}\Gamma_{\mathrm{DDE_A}} &= \frac{b_1^2 + b_2^2}{b^2}f(\delta, \Delta_1) + \frac{2b_1b_2}{b^2}(\Delta_1 + t_m)\\ &\approx \frac{b_1^2 + b_2^2 + 6b_1b_2}{3b^2}\Delta_1 + \frac{2b_1b_2}{b^2}t_m - \frac{b_1^2 + b_2^2}{9b^2}\delta,\end{aligned}$$

when $\Delta \gg \delta$. For symmetric DDE sequences, i.e., when $b_1 = b_2$, the corresponding exchange-weighted time is

$$\Gamma_{\mathrm{DDE_S}} = \frac{2}{3}\Delta_1 + \frac{1}{2}t_m - \frac{1}{18}\delta.$$

4. On the relation with FEXI-signal model

If the first pair of pulses of the asymmetric DDE sequence is fixed, then the dMRI signal can be normalized with respect to signal from the first SDE sequence as

$$\begin{aligned}&\ln S_{\mathrm{DDE_A}}(\cdot) - \ln S_{\mathrm{SDE}}(b_1, k\Delta_1)\\ &\approx (-\bar{D} + 2\mathrm{Var}(D)h_{\mathrm{DDE}}(k\Delta_1, kT)b_1)b_2\\ &\approx (-\bar{D} + 2\mathrm{Var}(D)(1 - k(\Delta_1 + t_m))b_1)b_2,\end{aligned} \tag{31}$$

where the last equation is obtained by using $h_{\mathrm{DDE}}(k\Delta_1, kT) \approx 1 - k(\Delta_1 + t_m)$.

A similar model was proposed in Ref. 12, which is given by

$$\begin{aligned}&\ln S_{\mathrm{FEXI}}(\cdot) - \ln S_{\mathrm{SDE}}(b_1, k\Delta_1)\\ &\approx -\bar{D}(1 - \sigma_f \exp(-\mathrm{AXR} \times t_m))b_2\\ &\approx (-\bar{D} + \bar{D}\sigma_f - \bar{D}\sigma_f t_m \mathrm{AXR})b_2.\end{aligned} \tag{32}$$

Since Δ_1 is fixed and t_m is changing in the experiment, the coefficients of t_m in Eqs. (31) and (32) should match with each other. Consequently we obtain

$$\begin{aligned}\bar{D}\sigma_f &= 2\mathrm{Var}(D)(1 - k\Delta_1)b_1,\\ \bar{D}\sigma_f \mathrm{AXR} &= 2\mathrm{Var}(D)kb_1.\end{aligned}$$

Thus, the following holds

$$\mathrm{AXR} = \frac{k}{1 - k\Delta_1}, \tag{33}$$

which is approximately equal to k if $k\Delta_1 \ll 1$. In the more general case, Eq. (33) can be applied to compute k using the estimated AXR and Δ_1.

E. Optimal sequence parameters

For the three sequences above, we will design the optimal acquisition parameters to maximize the sensitivity to water exchange. This will also allow for comparison of these sequences for practical applications. Optimality in this case is defined as the set of parameters that provide maximal signal decay due to water exchange. To obtain a fair comparison, we impose the following constraints on all the sequences: first, the diffusion time T is only allowed to change in the interval $[T_{\min}, T_{\max}]$; second, the maximal b-value has an upper bound $b_{\max}$. Thus, a natural constraint on Δ_1 in DDE experiments is $\Delta_1 \leq \frac{1}{2}T_{\min}$. We assume $T_{\min}$ is small so that the exchange sensitivity function $h_{\mathrm{SDE}}(kT_{\min}) \approx 1 - \frac{1}{3}kT_{\min}$. The attenuation due to exchange will be the objective function by which these sequences will be compared.

1. SDE sequences

From Eqs. (19) and (27), the dMRI signal for a SDE sequence is given by

$$\ln S_{\mathrm{SDE}}(b, kT) \approx -\bar{D}b + \frac{1}{2}\mathrm{Var}(D)h_{\mathrm{SDE}}(kT)b^2. \tag{34}$$

Thus, the maximal signal difference under the given constraints is approximately given by

$$e_{\mathrm{SDE}} = \frac{1}{2}\mathrm{Var}(D)(h_{\mathrm{SDE}}(kT_{\min}) - h_{\mathrm{SDE}}(kT_{\max}))b_{\max}^2. \quad (35)$$

If $kT_{\max} \gg 1$, i.e., if the exchange-sensitivity function $h_{\mathrm{SDE}}(kT_{\max}) \approx 0$, then

$$\begin{aligned} e_{\mathrm{SDE}} &\approx \frac{1}{2}\mathrm{Var}(D)h_{\mathrm{SDE}}(kT_{\min})b_{\max}^2 \\ &\approx \frac{1}{2}\mathrm{Var}(D)(1 - \frac{1}{3}kT_{\min})b_{\max}^2. \end{aligned} \quad (36)$$

On the other hand, if $kT_{\max} \ll 1$, i.e., if the exchange-sensitivity function $h_{\mathrm{SDE}}(kT_{\max}) \approx 1 - \frac{1}{2}kT_{\max}$, then

$$e_{\mathrm{SDE}} \approx \frac{1}{6}\mathrm{Var}(D)k(T_{\max} - T_{\min})b_{\max}^2. \quad (37)$$

2. DDE sequences

From Eqs. (19) and (30), the dMRI signal for asymmetric DDE sequence is given by

$$\begin{aligned} \ln S_{\mathrm{DDE_A}} \approx -\bar{D}b + \frac{1}{2}\mathrm{Var}(D)(&h_{\mathrm{SDE}}(k\Delta_1)(b_1^2 + b_2^2) \\ &+ 2b_1b_2h_{\mathrm{DDE}}(k\Delta_1, kT)). \end{aligned}$$

Thus, the signal difference for asymmetric DDE sequences is given by

$$e_{\mathrm{DDE_A}} \approx \mathrm{Var}(D)(h_{\mathrm{DDE}}(k\Delta_1, kT_{\min}) - h_{\mathrm{DDE}}(k\Delta_1, kT_{\max}))b_1b_2.$$

Moreover, the maximum value of the product b_1b_2 is equal to $\frac{1}{4}b_{\max}^2$, when $b_1 = b_2 = \frac{1}{2}b_{\max}$. In this case, the signal difference $e_{\mathrm{DDE_A}}$ is equal to the corresponding result with symmetric DDE sequences. Thus, we denote the signal difference for both types of DDE sequences as

$$e_{\mathrm{DDE}} = \frac{1}{4}\mathrm{Var}(D)(h_{\mathrm{DDE}}(k\Delta_1, kT_{\min}) - h_{\mathrm{DDE}}(k\Delta_1, kT_{\max}))b_{\max}^2. \quad (38)$$

If $kT_{\max} \gg 1$, i.e., $h_{\mathrm{DDE}}(k\Delta_1, kT_{\max}) \approx 0$, then

$$\begin{aligned} e_{\mathrm{DDE}} &\approx \frac{1}{4}\mathrm{Var}(D)h_{\mathrm{DDE}}(k\Delta_1, kT_{\min})b_{\max}^2 \\ &\approx \frac{1}{4}\mathrm{Var}(D)(1 - k(T_{\min} - \Delta_1))b_{\max}^2. \end{aligned}$$

Thus, the optimal value of Δ_1 that maximizes e_{DDE} is obtained when $\Delta_1 = \frac{1}{2}T_{\min}$. In this case,

$$e_{\mathrm{DDE}} \approx \frac{1}{4}\mathrm{Var}(D)(1 - \frac{1}{2}kT_{\min})b_{\max}^2. \quad (39)$$

On the other hand, if $kT_{\max} \ll 1$, then

$$e_{\mathrm{DDE}}(\cdot) \approx \frac{1}{4}\mathrm{Var}(D)k(T_{\max} - T_{\min})b_{\max}^2. \quad (40)$$

3. Comparing SDE and DDE sequences

If $kT_{\max} \gg 1$, then the maximum attenuation for SDE and DDE sequence is given by Eqs. (36) and (39), respectively. In this case,

$$e_{\mathrm{SDE}} > e_{\mathrm{DDE}}.$$

If $kT_{\max} \ll 1$, by comparing Eqs. (37) and (40), we obtain that

$$e_{\mathrm{SDE}} < e_{\mathrm{DDE}}.$$

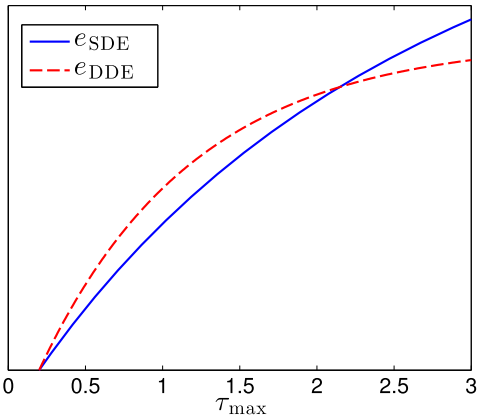

FIG. 2. A comparison of e_{SDE} and e_{DDE} from Eqs. (35) and (38), respectively, with $\tau_{\min} = 0.2$ and arbitrary values for $\mathrm{Var}(D)$ and $b_{\max}$. The plots show that $e_{\mathrm{DDE}} > e_{\mathrm{SDE}}$ for small $\tau_{\max}$, and $e_{\mathrm{DDE}} < e_{\mathrm{SDE}}$ for large $\tau_{\max}$.

Thus, e_{SDE} is less sensitive to k than e_{DDE} at short-time scale but has a stronger attenuation at long-time scale.

As an illustration of the above results, we plot e_{SDE}, e_{DDE} from Eqs. (35) and (38) for different values of $\tau_{\max}$ in Fig. 2 with a fixed value for $\tau_{\min}$ at $\tau_{\min} = 0.2$. The result shows that the DDE sequence has higher sensitivity than SDE sequence at short-time scales but has lower sensitivity at long-time scale.

III. EXPERIMENTS

We validated the proposed results using Monte Carlo simulations performed on a synthetic structure using a method similar to the approach described in Ref. 8. Figure 3 shows a partial field of view of the synthetic axonal packing structure used in our simulation, inset with illustration of the pulse sequences for simulating the dMRI signal. The axon diameter was fixed to 2.5 μm, and the intra- and extra-axonal volume

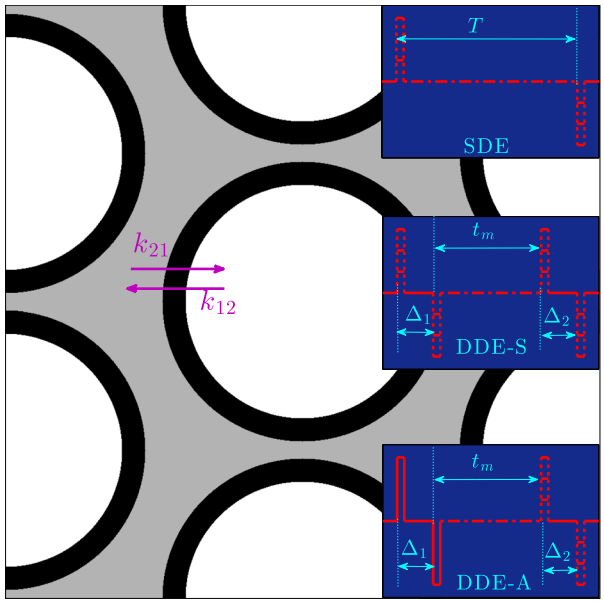

FIG. 3. Illustration of the synthetic tissue structure with permeable boundaries along with schematic for the SDE, $\mathrm{DDE_S}$, and $\mathrm{DDE_S}$ gradient sequences used for encoding the dMRI signals.

fractions were 0.7 and 0.3, respectively. The membrane permeability was chosen such that the effective intra-to-extra and extra-to-intra cellular exchange time was $t_{12} = \frac{1}{k_{12}} = 322$ ms (i.e., $k_{12} = 0.0031$ ms^{-1}) and $t_{21} = \frac{1}{k_{21}} = 139$ ms (i.e., $k_{21} = 0.0072$ ms^{-1}), respectively. These values fit in the range of exchange rates estimated from biological tissue.[31–33] The diffusivity of the spins was set to 3 μm^2/ms. Both SDE and DDE modulated signals were computed using the simulated diffusion trajectories. The pulse width for both sequences was fixed to 0.45 ms, and the diffusion or mixing time was changed for measuring the exchange rate. In the SDE experiments, the diffusion time was chosen in the interval $T \in [120, 240]$ ms, i.e., $T_{\min} = 120$ ms and $T_{\max} = 240$ ms, and $b_{\max} = 10$ ms/μm^2.

We also examined the signal due to symmetric and asymmetric DDE sequences, as shown in Fig. 3. For the symmetric DDE sequence, we applied the proposed result to set $\Delta_1 = \frac{T_{\min}}{2} = 60$ ms. For comparison, we also applied a non-optimal value for Δ_1 with $\Delta_1 = 30$ ms. For the asymmetric SDE sequence, we used the following optimal parameters: $\Delta_1 = 60$ ms and $b_1 = 5$ ms/μm^2. For comparison, we also used a non-optimal sequence with $b_1 = 2.5$ ms/μm^2.

The purpose of this experiment is (1) to examine the performance of the models in Eqs. (6) and (7) in fitting simulated signals and in estimating the water exchange rate, (2) to examine the cumulant expansion of SDE and DDE signals and compare them with the complete signal models, (3) to validate the optimality of the proposed experimental parameters, (4) to compare the signal differences, i.e., e_{SDE} and e_{DDE}, between SDE and DDE sequences under the same constraints.

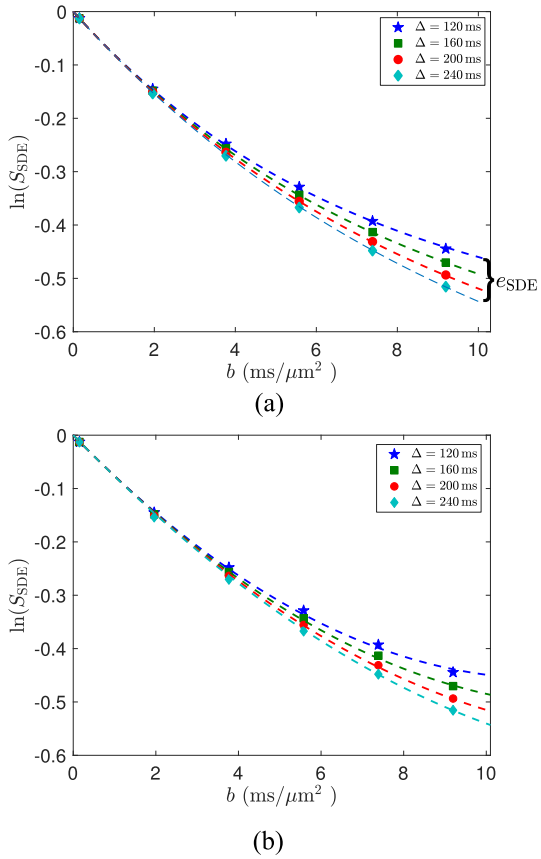

FIG. 4. The markers show the simulated SDE signal. The dashed lines in (a) show the estimated signals (S_{SDE}) using the complete signal model (6). (b) shows the estimated signals (S_{SDE}) using the cumulant expansion (19) with h_{SDE} given by (27).

IV. RESULTS

The dMRI signal for the SDE sequence is illustrated in Fig. 4, where the markers show the Monte Carlo simulated data, the dashed lines in Fig. 4(a) are the estimated signal using the complete signal model from (6), and Fig. 4(b) shows the signal using the cumulant expansion (19) with h_{SDE} given by (27). The closed-form expression for the matrix exponential $\exp(M(q)\Delta)$ in (6) is provided in Appendix A. The model parameters were estimated using the *lsqnonlin* algorithm implemented in MATLAB®. We note that the estimated signal in Fig. 4(a) fits nicely to the simulated data. The cumulant expansion in Fig. 4(b) has a slight fitting error at high b-values due to the truncation of higher order terms. The estimated model parameters in Fig. 4(a) were $D_1 = 0$ μm^2/ms, $D_2 = 0.2819$ μm^2/ms, $k_{12} = 0.0034$ ms^{-1}, and $k_{21} = 0.0080$ ms^{-1}. The estimated parameters for the cumulant expansion were $D_1 = 0.001$ μm^2/ms, $D_2 = 0.2067$ μm^2/ms, $k_{12} = 0.0040$ ms^{-1}, and $k_{21} = 0.0064$ ms^{-1}. Both are close to the true exchange rates. The estimated apparent diffusivity is much lower than the set value of intrinsic diffusivity, due to restrictions and hindrances from the tissue boundaries. We remark that these signals all have similar slopes near $b = 0$, which indicates that the apparent diffusivity is nearly constant at this time scale as shown in (12). Therefore, the assumption of constant diffusivity is valid in this experiment.

Figures 5(a) and 5(b) illustrate the simulated signal for symmetric DDE sequences with $\Delta_1 = 60$ ms using the complete signal model (7) and the cumulant expansion (19), respectively. We note that the cumulant expansion has slightly higher fitting error at high b-values. The estimated model parameters corresponding to Fig. 5(a) are $D_1 = 0.0130$ μm^2/ms, $D_2 = 0.3149$ μm^2/ms, $k_{12} = 0.0022$ ms^{-1}, and $k_{21} = 0.0064$ ms^{-1}. The estimated parameters for Fig. 5(a) are $D_1 = 0.0037$ μm^2/ms, $D_2 = 0.1955$ μm^2/ms, $k_{12} = 0.0028$ ms^{-1}, and $k_{21} = 0.0040$ ms^{-1}. The estimated exchange rates are slightly lower than the underlying true values.

Figure 5(c) illustrates the simulated and estimated signal using (7) with $\Delta_1 = 30$ ms, which is suboptimal according to the theoretical analysis in Sec. II E 2. The estimated model parameters were $D_1 = 0.0220$ μm^2/ms, $D_2 = 0.3369$ μm^2/ms, $k_{12} = 0.0012$ ms^{-1}, and $k_{21} = 0.0040$ ms^{-1}. We note that the signal variance is much smaller in Fig. 5(c) for the suboptimal condition compared to the optimal parameters in Fig. 5(a). This demonstrates the advantage of using optimized parameters for more sensitivity to exchange.

Figures 6(a) and 6(b) illustrate the simulated signal for asymmetric DDE sequences versus b_2 with b_1 fixed at $b_1 = 5$, and 2.5 ms/μm^2, respectively. The maximal b-value in both cases is equal to 10 ms/μm^2. Similar to the case of symmetric DDE sequences, the dashed lines are the estimated results from Eq. (7), which all fit nicely with the simulated data shown by the markers. The estimated model parameters corresponding to Fig. 6(a) are $D_1 = 0.0158$ μm^2/ms, $D_2 = 0.3675$ μm^2/ms, $k_{12} = 0.0028$ ms^{-1}, and $k_{21} = 0.0115$ ms^{-1}.

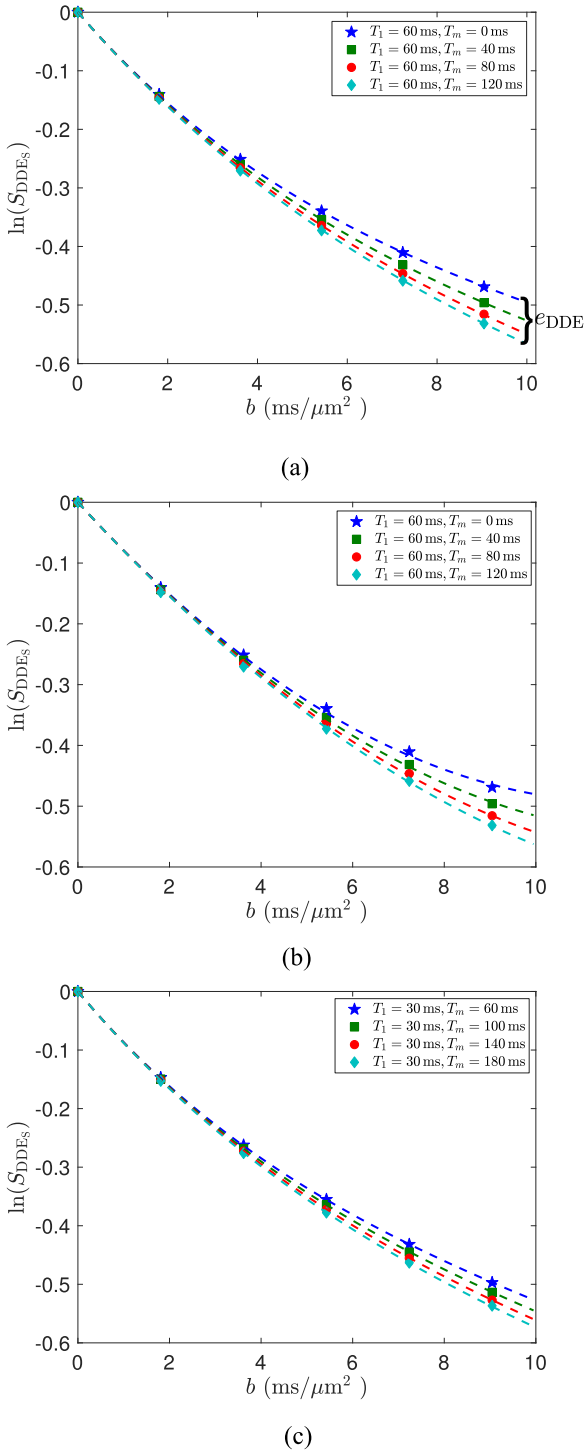

FIG. 5. The markers in (a) and (b) show the simulated signals using symmetric DDE sequences with the theoretically optimal $\Delta_1 = 60$ ms and the markers in (c) are the simulated signal with $\Delta_1 = 30$ ms. The dashed lines in (a) and (c) illustrate the estimated signals using the complete signal model (7). The dashed lines in (b) are estimated signals using the cumulant expansion (19) with $h(\cdot)$ given by (30).

The estimated model parameters for Fig. 6(b) are equal to $D_1 = 0\ \mu\text{m}^2/\text{ms}$, $D_2 = 0.2494\ \mu\text{m}^2/\text{ms}$, $k_{12} = 0.0043\ \text{ms}^{-1}$, and $k_{21} = 0.0085\ \text{ms}^{-1}$.

We note that the difference between signals, i.e., e_{DDE}, with $t_m = 120$ ms and $t_m = 0$ ms at $b_2 = 5\ \text{ms}/\mu\text{m}^2$ in Fig. 6(a) is equal to 0.0417, whereas the corresponding value from

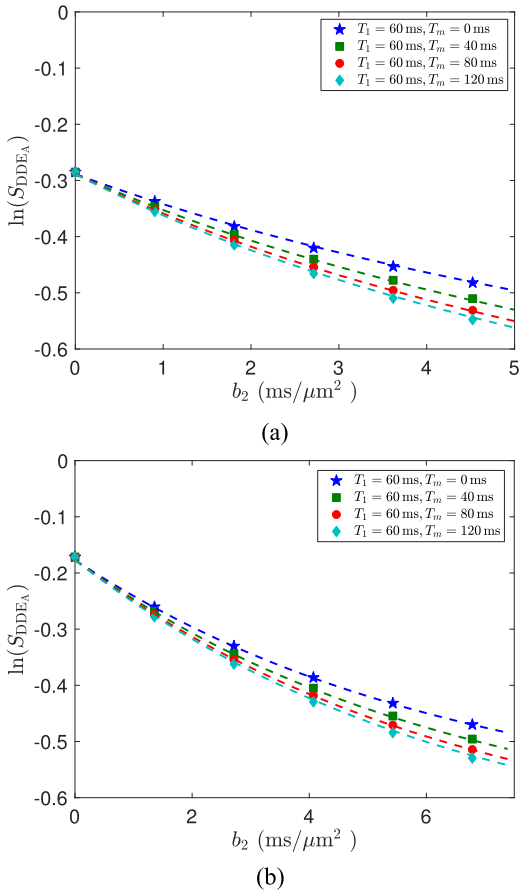

FIG. 6. The dashed lines in (a) show the estimated signal using symmetric DDE sequences with the theoretically optimal $b_1 = 10\ \text{ms}/\mu\text{m}^2$, which fit nicely to the signal from simulated data shown by the markers. Similarly, (b) shows the signals with a non-optimal value $b_1 = 5\ \text{ms}/\mu\text{m}^2$, which leads to a slightly weaker signal difference, i.e., e_{DDE}, compared to (a).

Fig. 6(b) at $b_2 = 7.5\ \text{ms}/\mu\text{m}^2$ has a smaller value at 0.0373, which supports the optimality of $b_1 = 5\ \text{ms}/\mu\text{m}^2$ in maximizing signal difference.

Figure 7 illustrates the comparison between e_{SDE} and e_{DDE} with the optimal parameters and the maximal diffusion time chosen in the interval $T_{\text{max}} \in [120, 240]$ ms. It

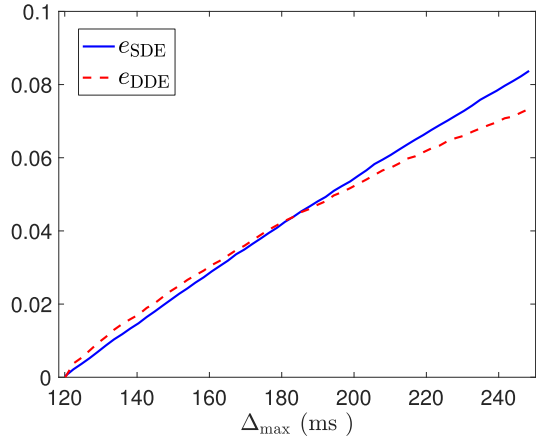

FIG. 7. A comparison of the signal differences e_{SDE} and e_{DDE} with $T_{\text{min}} = 120$ ms, $b_{\text{max}} = 20\ \text{ms}/\mu\text{m}^2$, and $T_{\text{max}} \in [120, 240]$ ms. This provides an experimental validation of the results from Fig. 2.

shows a very similar feature as in Fig. 2, though the theoretical analysis in Fig. 2 did not consider the third or higher order terms. More specifically, Fig. 7 shows that the signal change in a DDE sequence is more sensitive to water exchange than a SDE sequence when $\Delta_{\max}$ is small. But the SDE sequence provides larger signal changes at long time scale.

V. DISCUSSION AND CONCLUSIONS

In this paper, we investigated a model for the diffusion-and-exchange stochastic processes of water molecules. We derived a generalized expression of Kärger's model for the temporal evolution of the dMRI signal using any type of gradient sequence. We also derived analytical solutions for special case of SDE and DDE sequences. Moreover, we also proposed a novel solution for computing the cumulant expansion of dMRI signal using the stochastic evolution process without taking Taylor's series expansion from the complex signal models. Based on this general solution, we derived the cumulant expansion for the dMRI signal for SDE as well as symmetric and asymmetric DDE sequences. The cumulant expansions show that the water exchange rate is related to the linear coefficient of the b-value for asymmetric DDE sequences, whereas it involves the quadratic terms for SDE and symmetric DDE sequences. Moreover, the cumulant expansions also provide the exact relation between the AXR from the FEXI approach and the true water exchange rate.

From the cumulant expansions, we also computed the optimal parameters for the DDE sequences under realistic constraints on the b-values and diffusion time, in order to provide maximal signal difference for increased sensitivity to water exchange. For the symmetric DDE sequence, we showed that the optimal diffusion time Δ_1 should be set to its upper bound at $\frac{1}{2}T_{\min}$. For the asymmetric DDE sequences, the optimal value of b_1 is equal to $\frac{1}{2}b_{\max}$. Moreover, we also showed that the signal from a DDE sequence with optimal parameters is more sensitive to water exchange than the signal from the SDE sequence.

Finally, we note that a limitation of the present work is the assumption of constant diffusion coefficients for each compartment in the diffusion-exchange model. An important future direction is to explore the application of more realistic models that take into account restrictions or hindrances in the diffusion processes in situations with fast exchange rate. Moreover, generalizations to multiple components, anisotropic diffusivities, and vector-valued gradient waveforms, which are important for estimation of microscopic anisotropy,[34,35] will also be explored in our future work.

ACKNOWLEDGMENTS

This work was supported in part under Grant Nos. R21MH115280 (PI: Ning), R01MH097979 (PI: Rathi), R01MH111917 (PI: Rathi), R01MH074794 (PI: Westin), and P41EB015902 (PI: Kikinis), the Swedish Research Council (Grant No. 2016-03443), the Swedish Foundation for Strategic Research (Grant No. AM13-0090), and the CR Award (Grant No. MN15).

APPENDIX A: PROOF OF THE GENERALIZED KÄRGER MODEL IN SEC. II B

Without loss of generality, we will only derive the derivative $\frac{\partial S_1(q,t)}{\partial t}$. By definition,

$$S_1(q,t+\delta_t) = \sum_{j=1}^{2} p_j^{\infty} p_{j1}(t+\delta_t)\mathcal{E}(e^{\mathrm{i}\phi(t+\delta_t)} | s(t+\delta_t)=1, s(0)=j).$$

We denote $\phi(t,t+\delta_t) \coloneqq \int_t^{t+\delta_t} q(\tau)\sigma(\boldsymbol{x}(\tau))\eta(\tau)d\tau$. Then, it holds that $\phi(t+\delta_t)=\phi(t)+\phi(t,t+\delta_t)$ and $\phi(t)$ is independent of $\phi(t,t+\delta_t)$. Thus, it holds that

$$\begin{aligned} &S_1(q,t+\delta_t) \\ &\quad= \sum_{j=1}^{2}\sum_{k=1}^{2} p_j^{\infty} p_{jk}(t)p_{k1}(\delta_t)\mathcal{E}(e^{\mathrm{i}\phi(t)} \mid s(t)=k, s(t+\delta_t)=j) \\ &\qquad\times \mathcal{E}(e^{\mathrm{i}\phi(t,t+\delta_t)} \mid s(t+\delta_t)=1, s(t)=k) \\ &\quad= S_1(q,t)p_{11}(\delta_t)\mathcal{E}(e^{\mathrm{i}\phi(t,t+\delta_t)} \mid s(t+\delta_t)=1, s(t)=1) \\ &\qquad+ S_2(q,t)p_{21}(\delta_t)\mathcal{E}(e^{\mathrm{i}\phi(t,t+\delta_t)} \mid s(t+\delta_t)=1, s(t)=2). \end{aligned} \tag{A1}$$

By discretizing Eq. (2), we obtain that

$$\begin{aligned} p_{11}(\delta_t) &= p_{11}(0)(1-k_{12}\delta_t) + p_{12}(0)k_{21}\delta_t + o(\delta_t) \\ &= 1 - k_{12}\delta_t + o(\delta_t). \end{aligned}$$

To derive $\mathcal{E}(e^{\mathrm{i}\phi(t,t+\delta_t)} \mid s(t+\delta_t)=1, s(0)=1)$, we define the event $\mathcal{A}(t,\delta_t) \coloneqq \{\exists t_1 \in [t,t+\delta_t] \text{ s.t. } s(t_1)\neq s(t)\}$, i.e., $\mathcal{A}(t,\delta_t)$ denotes the event that water exchange happens during the interval $[t,t+\delta_t]$ with given boundary conditions $s(t)=1$, $s(t+\delta)=1$. Let $\mathcal{A}^c(t,\delta_t)$ denote the complementary event to $\mathcal{A}(t,\delta_t)$. Using Bayes' rule, we obtain that

$$\begin{aligned} &\mathcal{E}(e^{\mathrm{i}\phi(t,t+\delta_t)} \mid s(t+\delta_t)=1, s(t)=1) \\ &\quad= \mathrm{Prob}(\mathcal{A}(t,\delta_t) \mid s(t)=1, s(t+\delta_t)=1)\mathcal{E}(e^{\mathrm{i}\phi(t,t+\delta_t)} \mid s(t+\delta_t)=1, s(t)=1, \mathcal{A}(t,\delta_t)) \\ &\qquad+ \mathrm{Prob}(\mathcal{A}^c(t,\delta_t) \mid s(t)=1, s(t+\delta_t)=1)\times\mathcal{E}(e^{\mathrm{i}\phi(t,t+\delta_t)} \mid s(t+\delta_t)=1, s(t)=1, \mathcal{A}^c(t,\delta_t)). \end{aligned}$$

We note that, for short δ_t, the probability of exchange during the interval $[t,\ t+\delta_t]$ with the boundary condition that $s(t+\delta_t)=1$, $s(t)=1$ is about zeros, i.e.,

$$\mathrm{Prob}(\mathcal{A}(t,\delta_t) \mid s(t)=1, s(t+\delta_t)=1) = \frac{\mathrm{Prob}(s(t+\delta_t)=1 \mid s(t)=1) - \mathrm{Prob}(\mathcal{A}^c(t,\delta_t) \mid s(t)=1)}{\mathrm{Prob}(s(t+\delta_t)=1 \mid s(t)=1)}$$

is of order $o(\delta_t)$. Moreover,

$$\mathcal{E}(e^{i\phi(t,t+\delta_t)} \mid s(t+\delta_t)=1, s(t)=1, \mathcal{A}^c(t,\delta_t)) = \exp(-\int_t^{t+\delta_t} q(\tau)^2 ds D_1) = 1 - q(t)^2 D_1 \delta_t + o(\delta_t).$$

Thus,

$$p_{11}(\delta_t)\mathcal{E}(e^{i\phi(t,t+\delta_t)} \mid s(t+\delta_t)=1, s(t)=1) = 1 - (k_{12} + q(t)^2 D_1)\delta_t + o(\delta_t). \quad \text{(A2)}$$

Similarly, we can show that

$$p_{21}(\delta_t)\mathcal{E}(e^{i\phi(t,t+\delta_t)} \mid s(t+\delta_t)=1, s(t)=2) = k_{21}\delta_t + o(\delta_t). \quad \text{(A3)}$$

By substituting Eqs. (A2) and (A3) into Eq. (A1), we can prove Eq. (5).

APPENDIX B: THE CLOSED-FORM EXPRESSION FOR SDE SIGNAL

For completeness, we provide the closed-form expression for the matrix-exponential function used for computing the SDE and DDE signals, which is given by

$$\exp(M(q)t) = \begin{bmatrix} S_{11}(q,t) & S_{21}(q,t) \\ S_{12}(q,t) & S_{22}(q,t) \end{bmatrix},$$

where

$$S_{11}(q,t) = -\frac{-q^2D_1 - k_{12} + q^2D_B}{q^2(D_A - D_B)} e^{-q^2D_A t} + \frac{-q^2D_1 - k_{12} + q^2D_A}{q^2(D_A - D_B)} e^{-q^2D_B t},$$

$$S_{12}(q,t) = \frac{(-q^2D_1 - k_{12} + q^2D_A)(-q^2D_1 - k_{12} + q^2D_B)}{k_{21}q^2(D_A - D_B)} \times (e^{-q^2D_A t} - e^{-q^2D_B t}),$$

$$S_{21}(q,t) = \frac{-k_{21}}{q^2(D_A - D_B)} (e^{-q^2D_A t} - e^{-q^2D_B t}),$$

$$S_{22}(q,t) = \frac{-q^2D_1 - k_{12} + q^2D_A}{q^2(D_A - D_B)} e^{-q^2D_A t} - \frac{-q^2D_1 - k_{12} + q^2D_B}{q^2(D_A - D_B)} e^{-q^2D_B t},$$

$$D_{A,B} = \frac{1}{2}\left(D_1 + D_2 + \frac{k_{12} + k_{21}}{q^2} \mp \sqrt{\left[D_1 + D_2 + \frac{k_{12} - k_{21}}{q^2}\right]^2 + \frac{4k_{12}k_{21}}{q^4}}\right).$$

These equations are essentially Kärger's signal models in Ref. 1, which can also be used to derive the closed-form solution for DDE signals. The closed-form models were used in the experiments to fit the simulated signals.

APPENDIX C: ON THE HIGHER-ORDER MOMENTS

Following a similar computational approach as used in the fourth order moment, we provide a general expression for the higher order moments $\mathcal{E}(\phi^{2n}(T))$ for $n \geq 2$ as follows:

$$\mathcal{E}(\phi^{2n}(T)) = (2n-1)!! \int_0^T \cdots \int_0^T \left(\prod_{i=1}^n q_{t_i}^2\right) \times \mathcal{E}(\prod_{i=1}^n \sigma(\boldsymbol{x}_{t_i})^2) dt_1 \ldots dt_n.$$

Assuming $t_1 \leq t_2 \cdots \leq t_n$,

$$2^{-n}\mathcal{E}(\prod_{i=1}^n \sigma(\boldsymbol{x}_{t_i})^2) = \sum_{k,i_1,\ldots,i_n=1}^{2} p_k^{\infty}\Big(p_{ki_1}(t_1)p_{i_1i_2}(t_2 - t_1) \ldots p_{i_{n-1}i_n}(t_n - t_{n-1}) \times \prod_{\ell=1}^n D_{i_\ell}\Big),$$

which provides the high-order autocorrelations of the diffusivities.

[1] J. Kärger, "NMR self-diffusion studies in heterogeneous systems," Adv. Colloid Interface Sci. **23**, 129–148 (1985).
[2] W. Price, A. Barzykin, K. Hayamizu, and M. Tachiya, "A model for diffusive transport through a spherical interface probed by pulsed-field gradient NMR," Biophys. J. **74**, 2259–2271 (1998).
[3] P. T. Callaghan, *Principles of Nuclear Magnetic Resonance Microscopy* (Clarendon Press, Oxford, 1991), Vol. 3.
[4] L. Ning, E. Özarslan, C.-F. Westin, and Y. Rathi, "Precise inference and characterization of structural organization (PICASO) of tissue from molecular diffusion," NeuroImage **146**, 452–473 (2017).
[5] J. Kärger, "Der einfluß der zweibereichdiffusion auf die spinechodämpfung unter berücksichtigung der relaxation bei messungen mit der methode der gepulsten feldgradienten," Ann. Phys. **482**, 107–109 (1971).
[6] E. O. Stejskal and J. E. Tanner, "Spin diffusion measurements: Spin echoes in the presence of a time-dependent field gradient," J. Chem. Phys. **42**, 288–292 (1965).
[7] N. Shemesh, S. J. Jesperson, D. Alexander, Y. Cohen, I. Drobnjak, T. B. Dyrby, J. Finsterbusch, M. Koch, T. Kuder, F. Laun, M. Lawrenz, H. Lundell, P. Mitra, M. Nilsson, E. Özarslan, D. Topgaard, and C.-F. Westing, "Conventions and nomenclature for double diffusion encoding NMR and MRI," Magn. Reson. Med. **75**, 82–87 (2016).
[8] M. Nilsson, E. Alerstam, R. Wirestam, F. Støahlberg, S. Brockstedt, and J. Lätt, "Evaluating the accuracy and precision of a two-compartment Kärger model using Monte Carlo simulations," J. Magn. Reson. **206**, 59–67 (2010).
[9] E. Fieremans, D. Novikov, J. Jensen, and J. Helpern, "Monte Carlo study of a two-compartment exchange model of diffusion," NMR Biomed. **23**, 711–724 (2010).
[10] P. Callaghan and I. Furó, "Diffusion-diffusion correlation and exchange as a signature for local order and dynamics," J. Chem. Phys. **120**, 4032–4038 (2004).
[11] I. Åslund, A. Nowacka, M. Nilsson, and D. Topgaard, "Filter-exchange PGSE NMR determination of cell membrane permeability," J. Magn. Reson. **200**, 291–295 (2009).

[12]S. Lasič, M. Nilsson, J. Lätt, F. Ståhlberg, and D. Topgaard, "Apparent exchange rate mapping with diffusion MRI," Magn. Reson. Med. **66**, 356–365 (2011).
[13]M. Nilsson, J. Lätt, D. van Westen, S. Brockstedt, S. Lasič, F. Ståhlberg, and D. Topgaard, "Noninvasive mapping of water diffusional exchange in the human brain using filter-exchange imaging," Magn. Reson. Med. **69**, 1572–1580 (2013).
[14]B. Lampinen, F. Szczepankiewicz, D. van Westen, E. Englund, P. Sundgren, J. Lätt, F. Støahlberg, and M. Nilsson, "Optimal experimental design for filter exchange imaging: Apparent exchange rate measurements in the healthy brain and in intracranial tumors," Magn. Reson. Med. **77**, 1104–1114 (2017).
[15]S. Lasič, S. Oredsson, S. Partridge, L. Saal, D. Topgaard, M. Nilsson, and K. Bryskhe, "Apparent exchange rate for breast cancer characterization," NMR Biomed. **29**, 631–639 (2016).
[16]F. Schilling, S. Ros, D. Hu, P. D'Santos, S. McGuire, R. Mair, A. Wright, E. Mannion, R. Franklin, A. Neves, and K. Brindle, "MRI measurements of reporter-mediated increases in transmembrane water exchange enable detection of a gene reporter," Nat. Biotechnol. **35**, 75–80 (2017).
[17]S. Lasič, H. Lundel, H. Topgaard, and T. Dyrby, "Effects of imaging gradients in sequences with varying longitudinal storage time-case of diffusion exchange imaging," Magn. Reson. Med. **79**(4), 2228–2235 (2017).
[18]D. S. Novikov, J. H. Jensen, J. A. Helpern, and E. Fieremans, "Revealing mesoscopic structural universality with diffusion," Proc. Natl. Acad. Sci. U. S. A. **111**, 5088–5093 (2014).
[19]S. N. Jespersen, J. L. Olesen, B. Hansen, and N. Shemesh, "Diffusion time dependence of microstructural parameters in fixed spinal cord," NeuroImage (published online, 2017).
[20]P. P. Mitra, P. N. Sen, and L. M. Schwartz, "Short-time behavior of the diffusion coefficient as a geometrical probe of porous media," Phys. Rev. B **47**, 8565 (1993).
[21]D. S. Novikov, E. Fieremans, J. H. Jensen, and J. A. Helpern, "Random walks with barriers," Nat. Phys. **7**, 508–514 (2011).
[22]L. Ning, K. Setsompop, C.-F. Westin, and Y. Rathi, "New insights about time-varying diffusivity and its estimation from diffusion MRI," Magn. Reson. Med. **78**, 763–774 (2016).
[23]E. O. Stejskal, "Use of spin echoes in a pulsed magnetic-field gradient to study anisotropic, restricted diffusion and flow," J. Chem. Phys. **43**, 3597–3603 (1965).
[24]G. E. Uhlenbeck and L. S. Ornstein, "On the theory of the Brownian motion," Phys. Rev. **36**, 823–841 1930.
[25]T. Miyaguchi, T. Akimoto, and E. Yamamoto, "Langevin equation with fluctuating diffusivity: A two-state model," Phys. Rev. E **94**, 012109 (2016).
[26]T. Akimoto and E. Yamamoto, "Distributional behaviors of time-averaged observables in the Langevin equation with fluctuating diffusivity: Normal diffusion but anomalous fluctuations," Phys. Rev. E **93**, 062109 (2016).
[27]V. Kiselev, "The cumulant expansion: An overarching mathematical framework for understanding diffusion NMR," in *Diffusion MRI: Theory, Methods, and Applications*, edited by D. K. Jones (Oxford University Press, Oxford, 2011), pp. 152–168.
[28]L. Ning, C.-F. Westin, and Y. Rathi, "Estimation of bounded and unbounded trajectories in diffusion MRI," Front. Neurosci. **10**, 129 (2016).
[29]J. H. Jensen, J. A. Helpern, A. Ramani, H. Lu, and K. Kaczynski, "Diffusional kurtosis imaging: The quantification of non-Gaussian water diffusion by means of magnetic resonance imaging," Magn. Reson. Med. **53**, 1432–1440 (2005).
[30]J. Lee and C. Springer, "Effects of equilibrium exchange on diffusion-weighted NMR signals: The diffusigraphic 'shutter-speed,'" Magn. Reson. Med. **49**, 450–458 (2003).
[31]G. Stanisz, G. Wright, M. Henkelman, and A. Szafer, "An analytical model of restricted diffusion in bovine optic nerve," Magn. Reson. Med. **37**, 103–111 (1997).
[32]C. Meier, W. Dreher, and D. Leibfritz, "Diffusion in compartmental systems. II. Diffusion-weighted measurements of rat brain tissue *in vivo* and postmortem at very large b-values," Magn. Reson. Med. **50**, 510–551 (2003).
[33]C. S. Landis, X. Li, F. W. Telang, P. E. Molina, I. Palyka, G. Vetek, and C. S. Springer, "Equilibrium transcytolemmal water-exchange kinetics in skeletal muscle *in vivo*," Magn. Reson. Med. **42**, 467–478 (1999).
[34]S. Lasič, F. Szczepankiewicz, S. Eriksson, M. Nilsson, and D. Topgaard, "Microanisotropy imaging: Quantification of microscopic diffusion anisotropy and orientational order parameter by diffusion MRI with magic-angle spinning of the q-vector," Front. Phys. **2**, 11 (2014).
[35]C.-F. Westin, H. Knutsson, O. Pasternak, F. Szczepankiewicz, E. Özarslan, D. van Westen, C. Mattisson, M. Bogren, L. J. O'Donnel, M. Kubicki, D. Topgaard, and M. Nilsson, "Q-space trajectory imaging for multidimensional diffusion MRI of the human brain," NeuroImage **135**, 345–162 (2016).